Earthq Eng & Eng Vib (2016) 15: 445-455 **DOI**: 10.1007/s11803-016-0335-z

A note on the surface motion of a semi-cylindrical canyon for incident cylindrical SH waves radiated by a finite fault

Reza S. Jalali† and Zaniar Tokmechi‡

Department of Civil Engineering, Faculty of Engineering, University of Guilan, P.O. Box 3756, Rasht, Iran

Abstract: The plane-wave assumption for incident SH waves can be a good approximation for cylindrical and spherical waves radiated from finite sources, even when the source is as close as twice the size of the inhomogeneity, and when the source and the inhomogeneity are described within the same coordinate system. However, in a more general setting, and when the fault's radiation pattern must be considered, the plane-wave approximation may not yield satisfactory answers for arbitrary orientation of the fault. Jalali *et al*. (2015) demonstrated this for a semi-cylindrical, sedimentary valley, and in this study we extend their results to a case in which the semi-circular, sedimentary valley is replaced by a canyon. We describe the effects of incident cylindrical waves on the amplitudes of surface motion in and near the semi-cylindrical canyon when the causative faults are at different distances and have different curvatures and orientations.

Keywords: plane SH waves; cylindrical SH waves; effects of arbitrary fault orientation on amplification of surface motions

1 Introduction

This paper is a continuation of the work by Jalali *et al*. (2015), in which the surface motions within and near a semi-cylindrical valley were studied for excitation by cylindrical waves radiated from finite faults that had arbitrary orientations. In this paper, for the same excitation, we analyze the motion in the vicinity of a semi-cylindrical canyon.

Most published papers on the amplification of incident waves by surface topography are based on the assumption that excitation can be described in terms of plane harmonic waves (e.g., Chen *et al*. 2008, 2011, 2012; Gao *et al*. 2012; Moeen-Vaziri and Trifunac 1985; Sanchez-Sesma 1983, 1985, 1990; Sanchez-Sesma and Rosenblueth 1979; Sanchez-Sesma *et al*. 2002; Trifunac 1973; Wong 1982; Wong and Trifunac 1974; Wong *et al*. 1977; Zhang *et al*. 2012a,b) while the studies of near field effects in terms of cylindrical waves are rare (Gao and Zhang, 2013). Most of these studies also assumed periodic excitation and presented the results in terms of transfer-function amplitudes both along the ground surface and in the vicinity of the inhomogeneity. This work has shown (1) how two- and three-dimensional interferences, scattering, and diffraction of linear plane waves by inhomogeneities lead to changes in the amplitudes and locations of the observed peaks of transfer functions for motions on the ground surface; and (2) the relative significance of the surface topography vs. interior material inhomogeneities (sedimentary valleys) in shaping the overall amplification patterns on the ground surface (Wong *et al*. 1977). Sanchez-Sesma *et al*. (2002) presented a review of these studies up to 2002. More recently scattering and diffraction of incident SH waves by surface topography has been investigated by the null-field boundary integral equation method using degenerate kernels (Chen *et al*. 2011, 2012). In this approach the degenerate kernel function, which is also the fundamental solution, is expanded into series using the addition theorem.

As in our paper on excitation of a sedimentary valley (Jalali *et al*., 2015), the purposes of this note are (1) to show how the arbitrary fault orientation further compromises the plane-wave approximation, and (2) to provide some examples illustrating when and for what geometries plane waves may still continue to provide useful results. We will analyze this subject by comparing the transfer functions for incident plane waves with the transfer functions for excitation by cylindrical waves from a periodic, finite source of SH waves that has an arbitrary orientation.

2 The model

Figure 1 shows the two-dimensional model that is considered in this paper, which consists of a semi-

Correspondence to: Reza S. Jalali, Dept. of Civil Eng., Faculty of Eng., University of Guilan, P.O. Box 3756, Rasht, Iran
Tel: (+98) 131 669 0270; Fax: (+98) 131 669 0271
E-mail: saleh@guilan.ac.ir
†Assistant Professor; ‡PhD Candidate
Received October 6, 2014; **Accepted** July 5, 2015

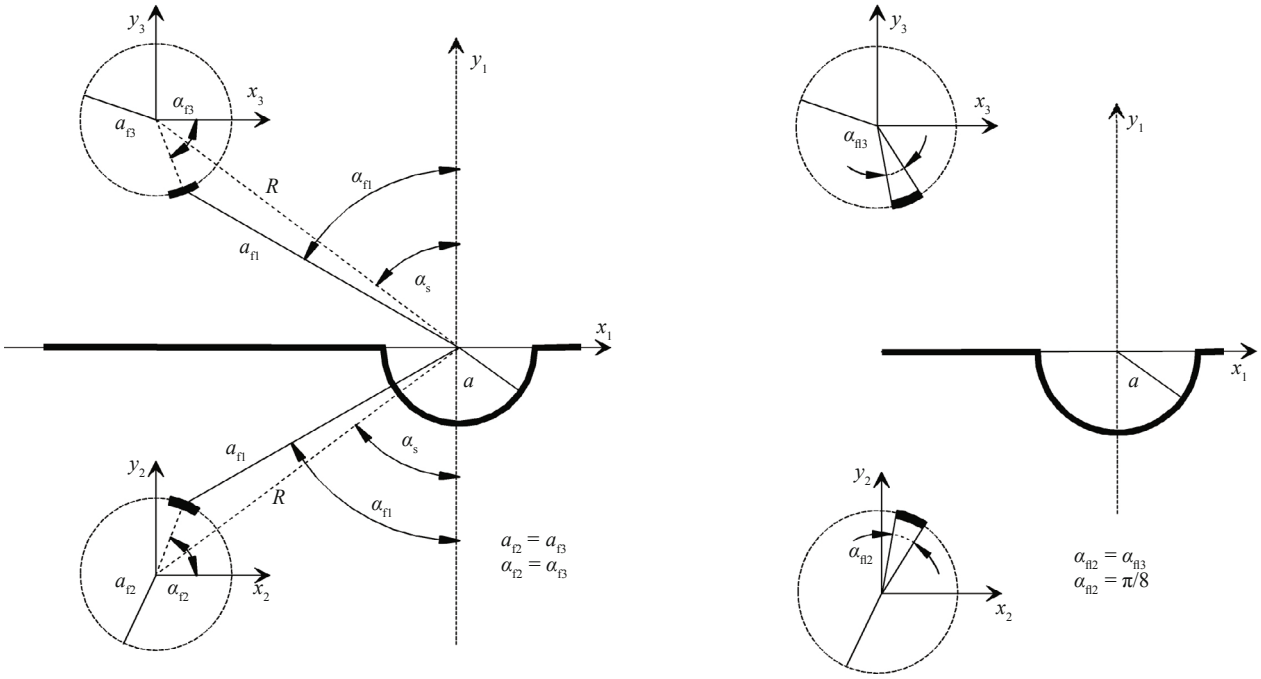

Fig. 1 Semi-cylindrical canyon

cylindrical canyon with radius a surrounded by an elastic homogeneous and isotropic half-space. We will use the parameter η to represent the ratio of a, the radius of the canyon, and $\lambda/2$, the half-wavelength of incident SH waves, in order to characterize dimensionless frequencies and wave-length ratios for the examples that will be shown in the following figures. The density and shear-wave velocity for the half-space are ρ_s and c_s, respectively. As is shown in the figure, another fault, symmetric with respect to the x-axis, is assumed and considered [$a_{f3} = a_{f2}$, $\alpha_{f3} = \alpha_{f2}$]. In coordinate system #1, the real fault is located at $r_1 = a_{f1}$. In coordinate system #2, the fault is located at $r_2 = a_{f2}$, between the angles $\alpha_{f2} - \alpha_{f12}/2$ and $\alpha_{f2} + \alpha_{f12}/2$, and the fault width is $a_{f2}\,\alpha_{f12}[\alpha_{f12} = \pi/8]$. In coordinate system #1, the imaginary fault is located at $r_1 = a_{f1}$. In coordinate system #3, the fault is located at $r_3 = a_{f3} = a_{f2}$, between the angles $2\pi - a_{f3} - \alpha_{f13}/2$ and $2\pi - a_{f3} + \alpha_{f13}/2$, and the fault width is $a_{f3}\,\alpha_{f13}[\alpha_{f13} = \pi/8]$.

To describe the periodic fault motion, in the coordinate systems #2 and #3 the boundary conditions along the circles $r_2 = a_{f2}$ and $r_3 = a_{f3}$ are taken to have dislocation amplitudes equal to one between $\alpha_{f2} - \alpha_{f12}/2$ and $\alpha_{f2} + \alpha_{f12}/2$, and between $\alpha_{f3} - \alpha_{f13}/2$ and $\alpha_{f3} + \alpha_{f13}/2$, and zero relative displacements elsewhere. The mathematical solution of the SH-wave radiation from the fault is presented in Appendix A. Except for differences in the boundary conditions along the canyon surface, this solution is analogous to the solution in Jalali *et al*. (2015) but we present it in Appendix A for completeness of presentation.

3 Results

Examples of computed amplification along the ground surface are illustrated in the next several figures. Figures 2 and 3 illustrate the effects of fault curvature (a_{f2}) on normalized surface-displacement amplitudes and phases when the distance between the fault and the canyon is $a_{f1} = 2a$, $4a$, and $16a$. As can be seen, when the fault is far from the canyon ($a_{f1} = 16a$) the effect of fault curvature on the surface-displacement amplitudes is small, and the plane-wave assumption can result in a fair approximation. But when the fault is as close as twice the size of the canyon, and for intermediate and large η, the effect of fault curvature begins to dominate, and the plane-wave assumption is no longer acceptable.

Because of geometric spreading, the cylindrical waves attenuate like $r^{-1/2}$, with distance r, while plane waves do not attenuate with r. To facilitate relative comparisons in this paper, all amplitudes of waves radiated from the fault have been normalized to produce the same average amplitudes inside the canyon as the average for the corresponding case with incident-plane waves. We compute these normalization factors by calculating the average spectral amplitudes of computed motions between $x_1/a = -1$ and $x_1/a = 1$. This was done to allow a more direct comparison of interference patterns of plane and cylindrical waves inside the canyon and its immediate vicinity. Figure 2 shows the amplification patterns for $a_{f1} = 16a$ (distant fault) while Fig. 3 shows the same for $a_{f1} = 2a$ (near fault). In Figs. 2 and 3, the left sides show symmetric amplitudes and phases for the fault directly beneath the canyon. The right sides of Figs. 2 and 3 show the amplifications and phases for a fault with $a_{f1} = 30^\circ$. The negative overall slope of the phase diagrams in these figures indicates wave propagation to the left, while the positive overall slope indicates propagation to right. The zones where this slope changes correspond to the projection onto the

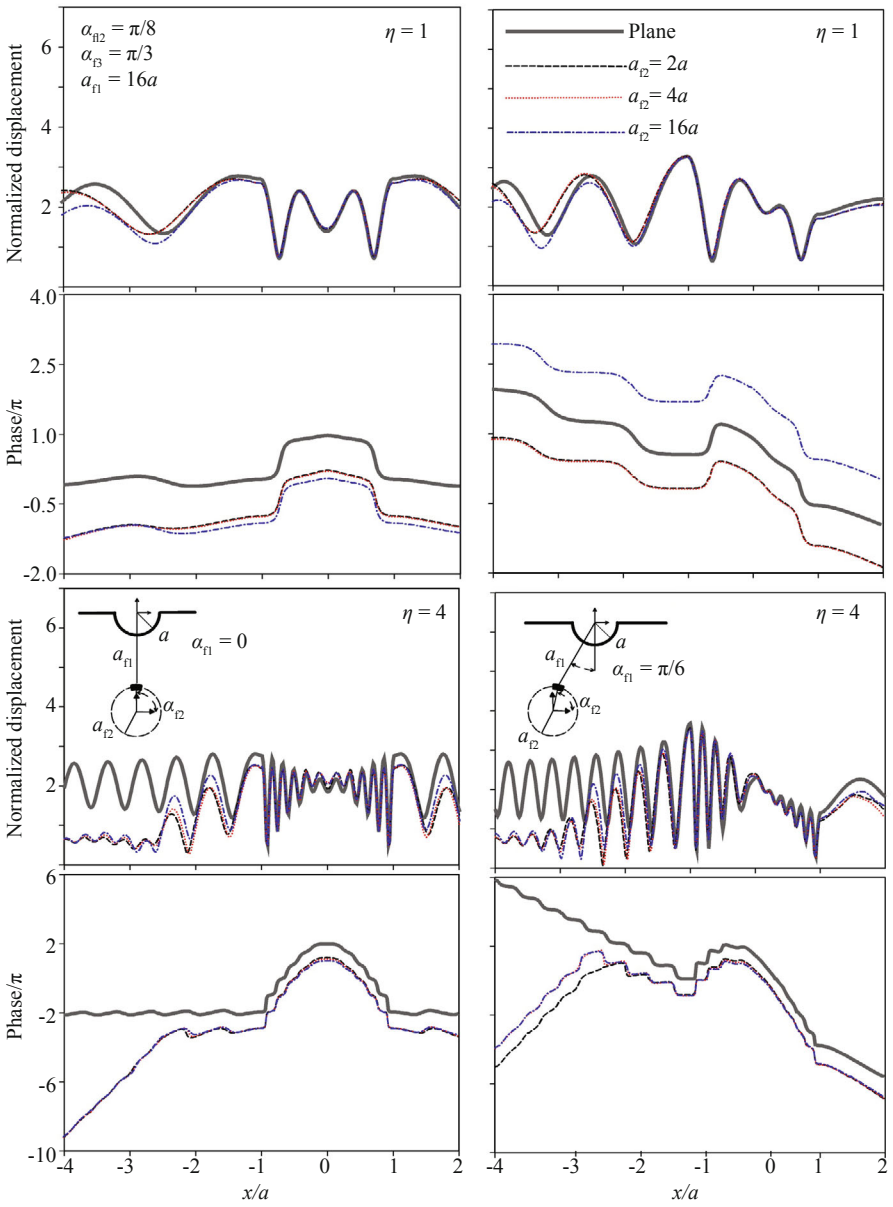

Fig. 2 Normalized displacement amplitudes and phases when $a_{f1} = 16a$, $\alpha_{f1} = 0, 30°$, and for different $a_{f2} = 2a, 4a, 16a$

ground surface of the sign changes in the fault radiation pattern. Since the cylindrical SH waves propagate away from the fault, with opposite signs of their amplitudes on the opposite sides of the fault, the amplitudes of the radiation pattern are largest in the radial direction, smallest in the transverse (tangential) direction of the fault and change the direction of propagation above and bellow the tangential directions.

Figure 4 shows the effect of fault curvature (a_{f2}) on normalized spectral amplification for two incident angles ($\alpha_{f1} = 0$, and $\pi/2 - \pi/16$) when $a_{f1} = 2a$. It shows how the changes in fault location and back scattering from the canyon walls can lead to large differences in spectral amplitudes. It also illustrates the effects of the shadow zone, behind the canyon, when the fault is at the surface and to the left of the canyon (cases 2 and 4). Here, we note again that the changes in a_{f2} result in the changes in the fault length. Therefore, for a_{f2} in all of the examples shown here the amplitudes of waves radiated from the fault have been normalized to agree with the average amplitudes inside the canyon for the case of incident-plane waves. This normalization facilitates comparison of the spectral amplification of cylindrical waves radiated from faults of different lengths, with the amplification computed for incident-plane waves inside and in the vicinity of the canyon. Thus, for example, in Fig. 4 (left), for $\alpha_{f1} = \pi/2 - \pi/16$ the amplitudes at $x/a = -1$ and -0.8 are larger than 4, which would correspond to the case for incident-plane waves with unit amplitude reflecting from the half-space (doubling the surface-displacement amplitudes) and then from the vertical wall of the quarter-space (again with doubling of the incident-wave amplitudes), with the end amplification being 4. For incident plane waves at $x/a = -1$, with increasing η , the

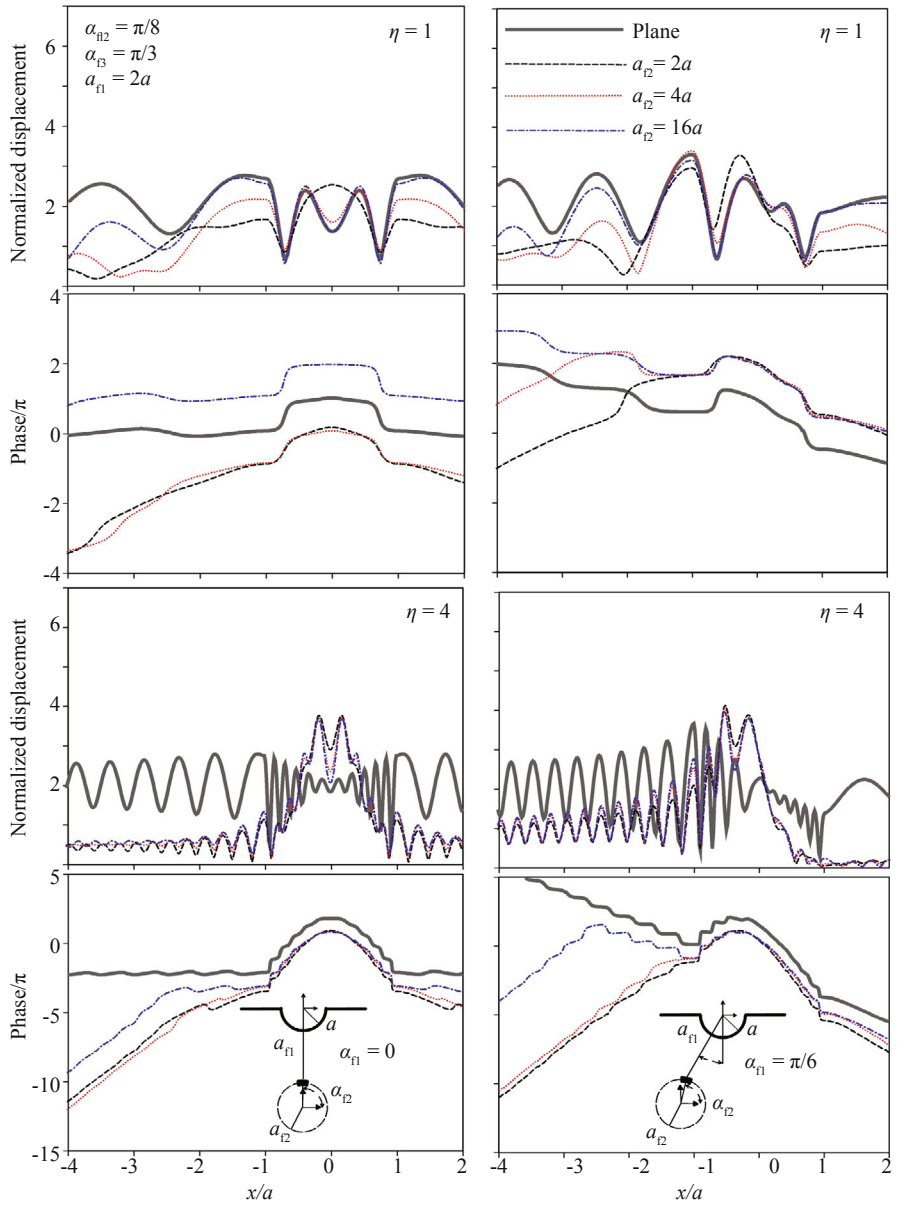

Fig. 3 Normalized displacement amplitudes and phases when $a_{f1} = 2a$, $\alpha_{f1} = 0, 30°$, and for different $a_{f2} = 2a, 4a, 16a$

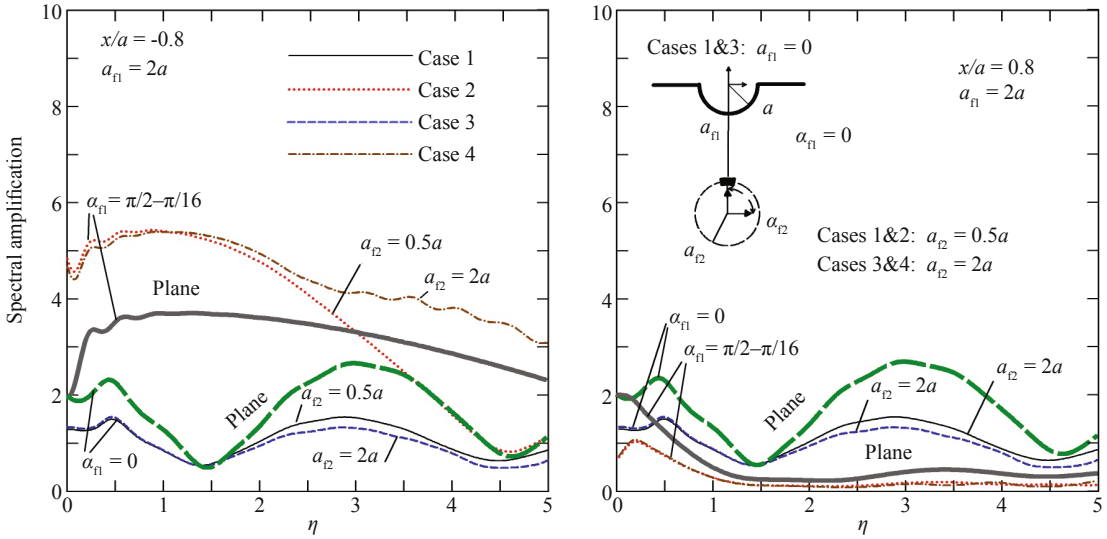

Fig. 4 Amplification at x/a = -1, -0.8, 0.8, and 1, for $a_{f1} = 2a$, and $a_{f2} = 0.5a$ and $2a$, when the source amplitudes are normalized to yield the same average amplitudes inside the canyon as for the incident-plane waves.

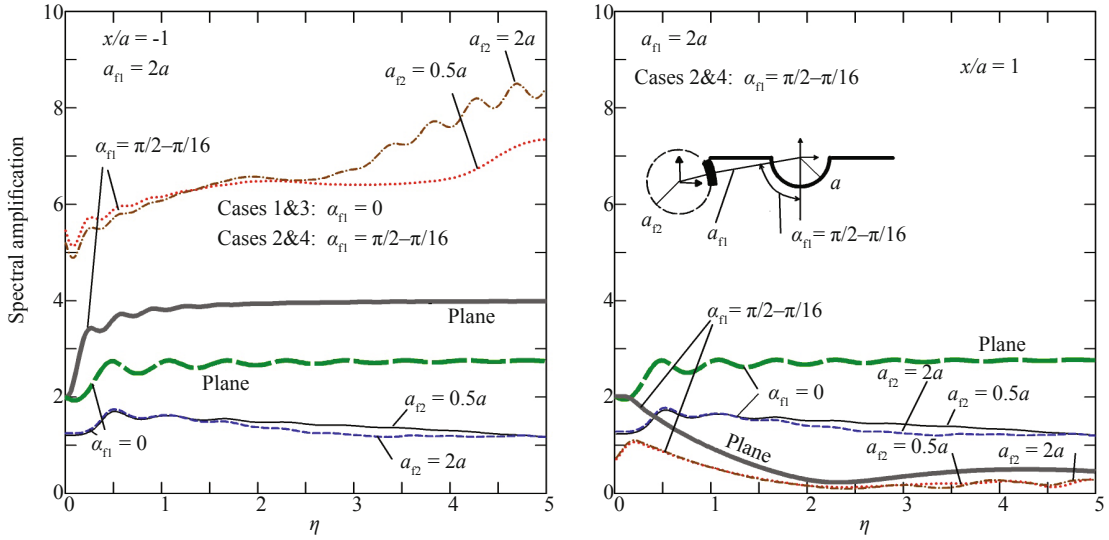

Fig. 4 Continued

amplification gradually increases toward 4. For $x/a = -0.8$ (a point inside the canyon and with an elevation lower than the half-space surface), the amplification begins to increase toward 4 for increasing η, but then it gradually decreases as the depth of that point approaches the quarter-wavelength of incident plane waves. As $\eta \to 0$, amplification of plane waves approaches 2 for all incidence angles, because very long waves cease to "see" the inhomogeneity represented by the canyon.

In Fig. 5(b), the position, curvature, and length of the fault are constant, but the fault rotates (see Fig. 5(a)). This figure shows the effects of the rotation of the radiation

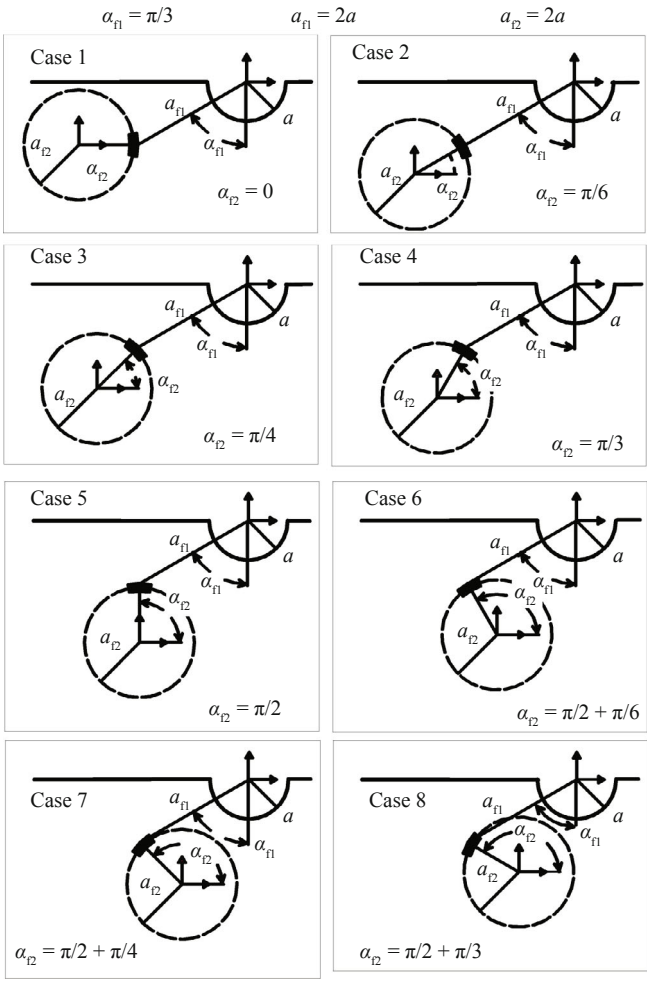

Fig. 5(a) Geometrical parameters for Cases 1–8, showing progressive changes to angle α_{f2}, which takes on the values of 0°, 30°, 45°, 60°, 90°, 120°, 135°, and 150°

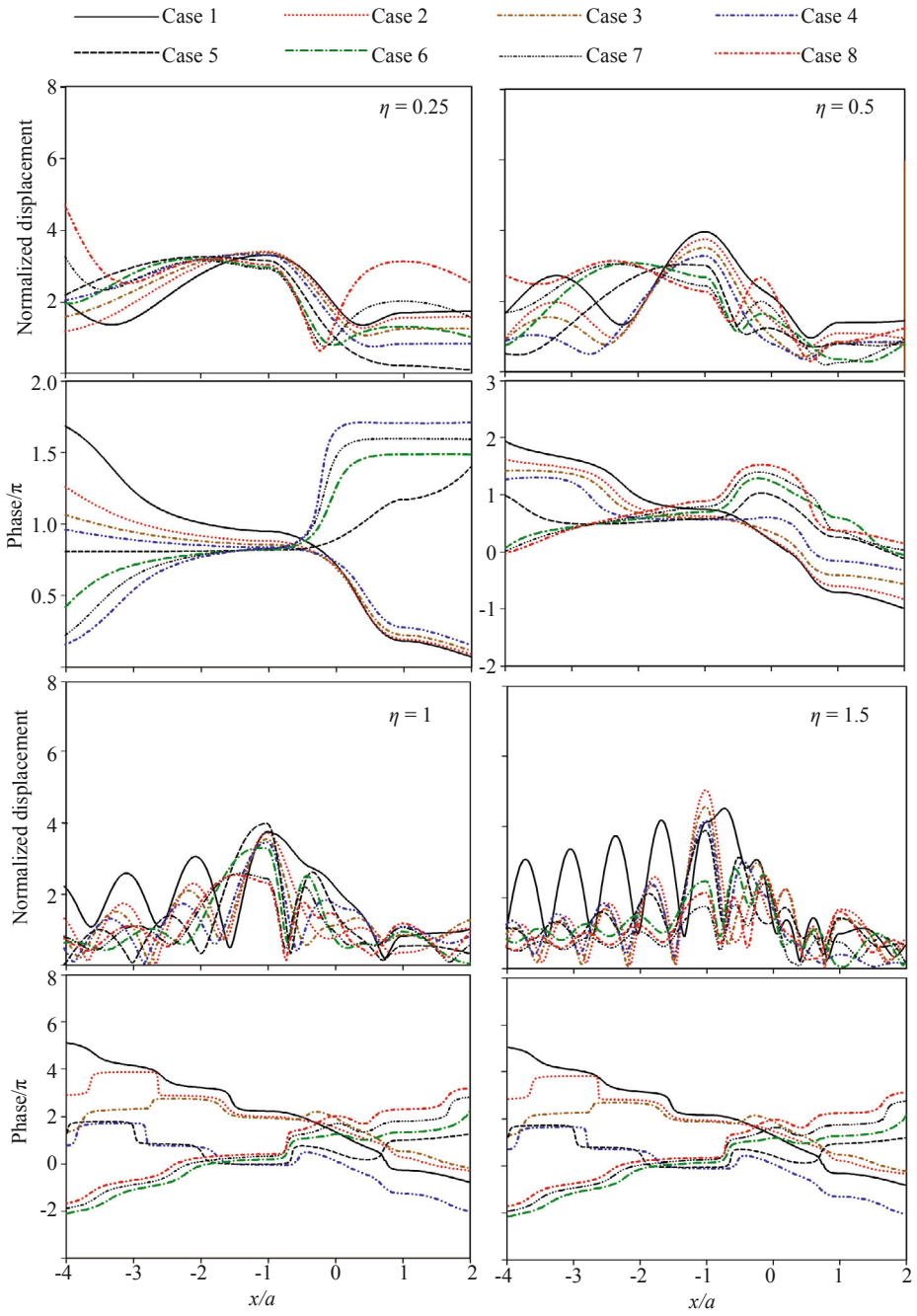

Fig. 5(b) Effects of the rotation of fault plane $\alpha_{f2} = 0°, 30°, 45°, 60°, 90°, 120°, 135°$, and 150° on normalized displacement amplitudes and phases for η = 0.25, 0.5, 1, and 1.5 and for $a_{f1} = \alpha_{f2} = 2a$, and $\alpha_{f1} = \pi/3$

pattern for the fault with normalized displacement amplitude and for different values of η when $a_{f1} = \alpha_{f2} = 2a$, and $\alpha_{f1} = \pi/3$.

4 Discussion and conclusions

In this note, we described an extension of the analysis by Jalali *et al*. (2015) and continued to examine the adequacy and the conditions for which the plane-wave representation can be used to describe excitation by cylindrical waves of inhomogeneities at the ground surface. We also presented examples of scattering and diffraction by a semi-cylindrical canyon with radius a. In addition, we also showed how the "addition theorem" in cylindrical coordinates can be used to study radiation from finite faults with general orientation and curvature. In the simplest terms, and in agreement with Jalali *et al*. (2015), we found that the plane waves can be used successfully to describe the excitation by cylindrical waves when the source is at a distance of at least several times the representative dimension of the inhomogeneity and when the normal to the fault surface is pointing in the direction of the inhomogeneity. This occurs when the direction of the maximum of the radiation pattern of the waves emanating from the fault is pointing

in the direction of the inhomogeneity and when the dimensionless frequency η is relatively small, say about one or less. Further details and interpretation of the results should be evident from the examples we have shown in the figures.

Rrferences

Chen JT, Chen PY and Chen CT (2008), "Surface Motion of Multiple Alluvial Valleys for Incident Plane SH-waves by Using a Semi-analytical Approach," *Soil Dynamics and Earthquake Engineering*, **28**: 58−72.

Chen JT, Lee JW and Shyu WS (2012), "SH Wave Scattering by a Semi-elliptical Hill Using Null-field Integral Equation Method and a Hybrid Method," *Geophysical Journal International*, **188**: 177−194.

Chen JT, Lee JW, Wu CF and Chen IL (2011), "SH-wave Diffraction by a Semi-circular Hill Revisited: a Null-field BoundaryIntegral Equation Method Using Degenerate Kernels," *Soil Dynamics and Earthquake Engineering*, **31**: 729−736.

Gao Y, Zhang N (2013), "Scattering of Cylindrical SH Waves Induced by a Symmetrical V-shaped Canyon: Near-source Topographic Effects," *Geophysical Journal International*, **193**(2): 874–885.

Gao Y, Zhang N, Li D, Liu H, Cai Y and Wu Y (2012), "Effects of Topographic Amplification Induced by a U-shaped Canyon on Seismic Waves," *Bulletin of the Seismological Society of America*, **102**(4): 1748–1763.

Jalali RS, Tokmechi Z and Trifunac MD (2015), "A Note on Surface Motion of a Semi-cylindrical Alluvial Valley for Incident-cylindrical SH Waves Radiating from a Fault with Arbitrary Orientation," *Soil Dynamics and Earthquake Engineering*, **79**: 80–88.

Moeen-Vaziri N and Trifunac MD (1985), "Scattering of Plane SH-waves by Cylindrical Canals of Arbitrary Shape," *Soil Dyn. Earthquake Eng.*, **4**: 18–23.

Sánchez-Sesma FJ (1983), "Diffraction of Elastic Waves by Three-dimensional Surface Irregularities," *Bull. Seism. Soc. Am.*, **73**: 1621–1636.

Sánchez-Sesma FJ (1985), "Diffraction of Elastic SH Waves by Wedges," *Bull. Seism. Soc. Am.*, **75**: 1435–1446.

Sánchez-Sesma FJ (1990), "Elementary Solutions for the Response of a Wedge-shaped Medium to Incident SH and SV Waves," *Bull. Seism. Soc. Am.*, **80**: 737–742.

Sánchez-Sesma FJ, Palencia VJ and Luzón F (2002), "Estimation of Local Site Effects during Earthquakes: An Overview," *ISET Journal of Earthquake Technology*, Paper No. 423, **39**(3): 167–193.

Sánchez-Sesma FJ and Rosenblueth E (1979), "Ground Motion at Canyons of Arbitrary Shape under Incident SH Waves," *Earthquake Eng. Struct. Dyn.*, **7**: 441–450.

Trifunac MD (1973), "Scattering of Plane SH Waves by a Semi-cylindrical Canyon," *Earthquake Eng. and Struct. Dyn.*, **1**: 267–281.

Wong HL (1982), "Effect of Surface Topography on the Diffraction of P, SV, and Rayleigh Waves," *Bull. Seism. Soc. Am.*, **72**: 1167–1183.

Wong HL and Trifunac MD (1974), "Scattering of Plane SH Wave by a Semi-elliptical Canyon," *Earthquake Eng. and Struct. Dyn.*, **3**: 157–169.

Wong HL, Trifunac MD and Westermo B (1977), Effects of Surface and Subsurface Irregularities on the Amplitudes of Monochromatic Waves," *Bull. Seism. Soc. Am.*, **67**: 353–368.

Zhang N, Gao Y, Cai Y, Li D and Wu Y (2012a), "Scattering of SH Waves Induced by a Nonsymmetrical V-shaped Canyon," *Geophysical Journal International*, **191**(1): 243−256.

Zhang N, Gao Y and Li D (2012b), "Scattering of SH Waves Induced by a Symmetrical V-shaped Canyon: a Unified Analytical Solution," *Earthquake Engineering and Engineering Vibration*, **11**(4): 445−460.

Appendix A

Figure 1 in the main text shows the two-dimensional model of the problem. As can be seen from the figure, the model consists of a semi-cylindrical canyon, with radius *a*, surrounded by an elastic homogeneous and isotropic half-space, where η is the ratio of a, the radius of the canyon, and $\lambda/2$, the half-wavelength of incident SH waves. The density and shear-wave velocity for the half-space are ρ_s and c_s, respectively. As can be seen, another symmetric fault with regard to the x-axis is assumed and considered [$a_{f3} = a_{f2}$, $\alpha_{f3} = \alpha_{f2}$].

In coordinate system #1, the real fault is located at $r_1 = a_{f1}$. In coordinate system #2, this fault is located at $r_2 = a_{f2}$, between the angles $\alpha_{f2} - \alpha_{f12}/2$ and $\alpha_{f2} + \alpha_{f12}/2$, and the fault width is a_{f2} α_{f12}[$\alpha_{f12} = \pi/8$].

In coordinate system #1, the imaginary fault is located at $r_1 = a_{f1}$. In coordinate system #3, this fault is located at $r_3 = a_{f3} = a_{f2}$, between the angles $2\pi - a_{f3} - \alpha_{f13}/2$ and $2\pi - a_{f3} + \alpha_{f13}/2$, and the fault width is a_{f3} α_{f13}[$\alpha_{f13} = \pi/8$].

Five displacement fields are defined to describe radiation from the fault, as follows:

(1) w_{sc}^1 for $a < r_1$ represents reflecting waves propagating from the canyon, (2) w_i^2 for $0 < r_2 < a_{f2}$ represents cylindrical waves propagating toward $r_2 = 0$, (3) w_o^2 for $a_{f2} < r_2$ represents cylindrical waves propagating away from $r_2 = 0$, (4) w_i^3 for $0 < r_3 < a_{f3}$ represents cylindrical waves propagating toward $r_3 = 0$, and (5) w_o^3 for $a_{f3} < r_3$ represents cylindrical waves propagating away from $r_3 = 0$.

In all regions, the out-of-plane SH waves can be achieved using the following equation:

$$\left(\frac{\partial^2}{\partial r^2}+\frac{1}{r}\frac{\partial}{\partial r}+\frac{1}{r^2}\frac{\partial^2}{\partial\theta^2}\right)U(r,\theta,t)=\frac{1}{c^2}\frac{\partial^2}{\partial t^2}U(r,\theta,t) \tag{A1}$$

The solution of the time-dependent field will be taken as harmonic, so that

$$U(r,\theta,t)=u(r,\theta)\mathrm{e}^{-\mathrm{i}\omega t} \tag{A2}$$

where ω is the angular frequency. Substituting Eq. (A2) into Eq. (A1) leads to

$$\left(\frac{\partial^2}{\partial r^2}+\frac{1}{r}\frac{\partial}{\partial r}+\frac{1}{r^2}\frac{\partial^2}{\partial\theta^2}\right)u(r,\theta)\mathrm{e}^{-\mathrm{i}\omega t}=-\frac{\omega^2}{c^2}u(r,\theta)\mathrm{e}^{-\mathrm{i}\omega t} \tag{A3}$$

Using the wave number $k=\omega/c$, we have

$$\left(\frac{\partial^2}{\partial r^2}+\frac{1}{r}\frac{\partial}{\partial r}+\frac{1}{r^2}\frac{\partial^2}{\partial\theta^2}+k^2\right)u(r,\theta)=0 \tag{A4}$$

When we assume that separation of the variables solves the problem $u(r,\theta)=R(r)\Theta(\theta)$, it follows that

$$\left(\frac{\partial^2}{\partial r^2}+\frac{1}{r}\frac{\partial}{\partial r}+\frac{1}{r^2}\frac{\partial^2}{\partial\theta^2}+k^2\right)R(r)\Theta(\theta)=0 \tag{A5a}$$

$$\left(\Theta(\theta)\frac{\partial^2R(r)}{\partial r^2}+\Theta(\theta)\frac{1}{r}\frac{\partial R(r)}{\partial r}+R(r)\frac{1}{r^2}\frac{\partial^2\Theta(\theta)}{\partial\theta^2}+R(r)\Theta(\theta)k^2\right)=0 \tag{A5b}$$

$$\left(\frac{r^2}{R(r)}\frac{\partial^2R(r)}{\partial r^2}+\frac{r}{R(r)}\frac{\partial R(r)}{\partial r}+\frac{1}{\Theta(\theta)}\frac{\partial^2\Theta(\theta)}{\partial\theta^2}+r^2k^2\right)=0 \tag{A5c}$$

$$\left(\frac{r^2}{R(r)}\frac{\partial^2R(r)}{\partial r^2}+\frac{r}{R(r)}\frac{\partial R(r)}{\partial r}+r^2k^2\right)=-\frac{1}{\Theta(\theta)}\frac{\partial^2\Theta(\theta)}{\partial\theta^2} \tag{A5d}$$

To solve Eq. (A5d), both sides of the equation should be equal to a constant. If this constant is chosen to be n^2, then

$$\left(\frac{r^2}{R(r)}\frac{\partial^2R(r)}{\partial r^2}+\frac{r}{R(r)}\frac{\partial R(r)}{\partial r}+r^2k^2\right)=-\frac{1}{\Theta(\theta)}\frac{\partial^2\Theta(\theta)}{\partial\theta^2}=n^2 \tag{A5e}$$

$$\left(\frac{\partial^2\Theta(\theta)}{\partial\theta^2}+\Theta(\theta)n^2\right)=0\Rightarrow\Theta(\theta)=\mathrm{e}^{\mathrm{i}n\theta} \tag{A5f}$$

$$\left(r^2\frac{\partial^2R(r)}{\partial r^2}+r\frac{\partial R(r)}{\partial r}+R(r)(r^2k^2-n^2)\right)=0 \tag{A5g}$$

and after variable transformation, $\xi=rk$,

$$\left(\frac{\partial R(r)}{\partial r}\right)=\left(\frac{\partial R(r)}{\partial\xi}\frac{\partial\xi}{\partial r}\right)=\frac{\partial R(r)}{\partial\xi}k \tag{A6a}$$

$$\frac{\partial}{\partial r}\left(\frac{\partial R(r)}{\partial r}\right)=\frac{\partial}{\partial r}\left(\frac{\partial R(r)}{\partial\xi}k\right)=\frac{\partial}{\partial\xi}\left(\frac{\partial R(r)}{\partial\xi}\right)\frac{\partial\xi}{\partial r}k=\frac{\partial^2R(r)}{\partial\xi^2}k^2 \tag{A6b}$$

$$\left(r^2\frac{\partial^2R(r)}{\partial\xi^2}k^2+r\frac{\partial R(r)}{\partial\xi}k+R(r)(r^2k^2-n^2)\right)=0 \tag{A6c}$$

$$\left(\xi^2\frac{\partial^2R(\xi/k)}{\partial\xi^2}+\xi\frac{\partial R(\xi/k)}{\partial\xi}+R(\xi/k)(\xi^2-n^2)\right)=0 \tag{A6d}$$

This is a Bessel differential equation, and its solution is

$$R(\xi/k)=C_n(\xi) \tag{A7}$$

Changing the variables again to $R_r=C_n(kr)$, the solution function will be $C_n(kr)\mathrm{e}^{\mathrm{i}n\theta}$. Since the solution has to be periodic in θ, n has to be an integer, and the solution is valid for all integer values of n, from minus infinity to plus infinity. Therefore, the general solution is a linear combination, as follows:

$$u(r,\theta)=\sum_{n=-\infty}^{\infty}A_nC_n(kr)\mathrm{e}^{\mathrm{i}n\theta} \tag{A8}$$

Using boundary conditions, the complex constants A_n can be determined. Depending on the physical condition of the problem, C_n is a Bessel function with order *n*, which can be either $J_n, Y_n, H_n^{(1)}$, or $H_n^{(2)}$. $H_n^{(1)}$ describes the outgoing waves, while $H_n^{(2)}$ describes the incoming waves. Because the series above is convergent, it is possible to truncate it into a finite sum with N terms, as follows:

$$u(r,\theta)=\sum_{n=-N}^{N}A_nC_n(kr)\mathrm{e}^{\mathrm{i}n\theta} \tag{A9}$$

The geometry of the model is suitable for using a cylindrical coordinate system, and therefore all formulas are presented depending on a cylindrical coordinate system r_i and θ_i (i = 1, 2, and 3). For determining the wave expansions of the different waves, relations are considered as follows (note that the superscripts of the wave names stand for the coordinate system number):

The scattering-wave expansion (coordinate system #1):

$$w_{\mathrm{sc}}^1=\sum_{n=-N}^{N}A_{\mathrm{sc},n}H_n^{(1)}(k_{\beta\mathrm{s}}r_1)\mathrm{e}^{\mathrm{i}n\theta_1} \tag{A10}$$

The wave expansion outside the coordinate system #2 circle (coordinate system #2):

$$w_{o2}^{2}=\sum_{n=-N}^{N}A_{o2,n}H_{n}^{(1)}(k_{\beta s}r_{2})e^{in\theta_{2}} \quad (A11)$$

The wave expansion inside the coordinate system #2 circle (coordinate system#2):

$$w_{i2}^{2}=\sum_{n=-N}^{N}A_{i2,n}J_{n}(k_{\beta s}r_{2})e^{in\theta_{2}} \quad (A12)$$

The wave expansion outside the coordinate system #3 circle (coordinate system#3):

$$w_{o3}^{3}=\sum_{n=-N}^{N}A_{o3,n}H_{n}^{(1)}(k_{\beta s}r_{3})e^{in\theta_{3}} \quad (A13)$$

The wave expansion inside the coordinate system #3 circle (coordinate system#3):

$$w_{i3}^{3}=\sum_{n=-N}^{N}A_{i3,n}J_{n}(k_{\beta s}r_{3})e^{in\theta_{3}} \quad (A14)$$

The mentioned waves must satisfy the boundary conditions as follows:

Zero stress on the flat surface leads to

$$B.1:\sigma_{\theta z}=\frac{\mu_{s}}{r_{1}}\frac{\partial(w_{o2}^{1}+w_{o3}^{1}+w_{sc}^{1})}{\partial\theta_{1}}\bigg|_{\theta_{1}=0,\pi}=0 \quad (A15)$$

$$B.2:\mu_{s}\frac{\partial(w_{o2}^{1}+w_{o3}^{1}+w_{sc}^{1})}{\partial r_{1}}\bigg|_{r_{1}=a}=0 \quad (A16)$$

The continuity of the stress in divided regions of coordinate system #2 is

$$B.3:\mu_{s}\frac{\partial w_{i2}^{2}}{\partial r_{2}}\bigg|_{r_{2}=a_{f2}}=\mu_{s}\frac{\partial(w_{o2}^{2}+w_{o3}^{2}+w_{sc}^{2})}{\partial r_{2}}\bigg|_{r_{2}=a_{f2}} \quad (A17)$$

The displacement difference in divided regions of coordinate system #2 is

$$B.4:w_{i2}^{2}\big|_{r_{2}=a_{f2}}-(w_{o2}^{2}+w_{o3}^{2}+w_{sc}^{2})\big|_{r_{2}=a_{f2}}=f_{1}(\theta_{2}) \quad (A18)$$

The continuity of the stress in divided regions of coordinate system #3 is

$$B.5:\mu_{s}\frac{\partial w_{i3}^{3}}{\partial r_{3}}\bigg|_{r_{3}=a_{f3}}=\mu_{s}\frac{\partial(w_{o2}^{3}+w_{o3}^{3}+w_{sc}^{3})}{\partial r_{3}}\bigg|_{r_{3}=a_{f3}} \quad (A19)$$

The displacement difference in divided regions of coordinate system #2 is

$$B.6:w_{i3}^{3}\big|_{r_{3}=a_{f3}}-(w_{o2}^{3}+w_{o3}^{3}+w_{sc}^{3})\big|_{r_{3}=a_{f3}}=f_{2}(\theta_{3}) \quad (A20)$$

For determining $f_1(\theta_2)$ and $f_2(\theta_3)$, we introduce $f(\theta)$ as follows:

$$f(\theta)=H[\theta-\alpha_{1}]-H[\theta-\alpha_{2}] \quad (A21)$$

where H is the Heaviside function, such that

$$H(\theta)=\begin{cases}0 & \theta<0\\ 1 & \theta\geq 0\end{cases} \quad (A22)$$

And $f_1(\theta_2)$ and $f_2(\theta_3)$ can be expressed as follows:

$$\begin{cases}f_{1}(\theta_{2})=f(\theta) & \theta=\theta_{2},\alpha_{1}=\alpha_{f2}-\alpha_{fl2}/2,\alpha_{2}=\alpha_{f2}+\alpha_{fl2}/2\\ f_{2}(\theta_{3})=f(\theta) & \theta=\theta_{3},\alpha_{1}=2\pi-\alpha_{f2}-\alpha_{fl2}/2,\alpha_{2}=2\pi-\alpha_{f2}+\alpha_{fl2}/2\end{cases} \quad (A23)$$

As can be seen from the boundary conditions, in order to solve the problem it is necessary to express radiated waves from the fault and its coordinate system into another coordinate system, which is suitable for application of the boundary conditions. Therefore, the addition theorems (Fig. A1) for the Bessel and Hankel functions are used to transfer the wave from the q-th coordinates to the p-th coordinates as follows (Esherbeni 1994; Esherbeni and Kishk 1992):

$$Z_{n}(k\rho_{q})e^{in\varphi_{q}}=\sum_{m=-\infty}^{\infty}J_{m}(k\rho_{p})Z_{m-n}(kd_{pq})e^{im\varphi_{p}}e^{-i(m-n)\varphi_{pq}} \quad (A24)$$

where

$$\begin{cases}\varphi_{pq}=\arccos\left(\dfrac{\rho'_{q}\cos(\varphi'_{q})-\rho'_{p}\cos(\varphi'_{p})}{d_{pq}}\right) & \text{if}:\rho'_{q}\sin(\varphi'_{q})\geq\rho'_{p}\sin(\varphi'_{p})\\ \varphi_{pq}=\arccos\left(\dfrac{\rho'_{p}\cos(\varphi'_{p})-\rho'_{q}\cos(\varphi'_{q})}{d_{pq}}\right) & \text{if}:\rho'_{q}\sin(\varphi'_{q})<\rho'_{p}\sin(\varphi'_{p})\end{cases} \quad (A25)$$

where (ρ'_q,φ'_q) and (ρ'_p,φ'_p) are the origin of the q-th and p-th coordinate systems, respectively, d_{pq} is the distance between the centers of the coordinate systems, and Z represents the Bessel or Hankel function.

As mentioned previously, the addition theorem is needed to satisfy the boundary conditions. Since we assume an imaginary fault, the zero-stress condition (boundary condition B.1) is satisfied automatically. Thus, it is just necessary to satisfy other boundary conditions using the addition theorem as follows.

Satisfying boundary condition B.2:

According to boundary condition B.2 (Eq. (A16)), we need to transfer all necessary waves from their original coordinate system to coordinate system #1. Using that,

and considering boundary condition B.2, leads to

$$\mu_{\mathrm{s}}\left[\sum_{n=-N}^{N} A_{\mathrm{sc},n} k_{\beta\mathrm{s}} \mathrm{H}_n'^{(1)}(k_{\beta\mathrm{s}} r_1)\mathrm{e}^{\mathrm{i}n\theta_1}\right] +$$
$$\mu_{\mathrm{s}}\left[\sum_{n=-N}^{N} A_{\mathrm{o}2,n} \sum_{m=-M}^{M} (k_{\beta\mathrm{s}} \mathrm{J}'_m(k_{\beta\mathrm{s}} r_1)\mathrm{H}_{m-n}^{(1)}(k_{\beta\mathrm{s}} R)\mathrm{e}^{\mathrm{i}m\theta_1}\mathrm{e}^{-\mathrm{i}(m-n)(\frac{3\pi}{2}-\alpha_{\mathrm{s}})})\right] +$$
$$\mu_{\mathrm{s}}\left[\sum_{n=-N}^{N} A_{\mathrm{o}3,n} \sum_{m=-M}^{M} (k_{\beta\mathrm{s}} \mathrm{J}'_m(k_{\beta\mathrm{s}} r_1)\mathrm{H}_{m-n}^{(1)}(k_{\beta\mathrm{s}} R)\mathrm{e}^{\mathrm{i}m\theta_1}\mathrm{e}^{-\mathrm{i}(m-n)(\frac{\pi}{2}+\alpha_{\mathrm{s}})})\right]_{r_1=a} = 0 \quad \text{(A26)}$$

Satisfying boundary condition B.3:

According to boundary condition B.3 (Eq. (A17)), we need to transfer all necessary waves from their original coordinate system to coordinate system #2. Using that, and considering boundary condition B.3, leads to

$$\mu_{\mathrm{s}}\left[\sum_{n=-N}^{N} A_{i2,n} k_{\beta\mathrm{s}} \mathrm{J}'_n(k_{\beta\mathrm{s}} r_2)\mathrm{e}^{\mathrm{i}n\theta_2}\right]_{r_2=a\mathrm{f}2} =$$
$$\mu_{\mathrm{s}}\left[\sum_{n=-N}^{N} A_{\mathrm{sc},n} \sum_{m=-M}^{M} (k_{\beta\mathrm{s}} \mathrm{J}'_m(k_{\beta\mathrm{s}} r_2)\mathrm{H}_{m-n}^{(1)}(k_{\beta\mathrm{s}} R)\mathrm{e}^{\mathrm{i}m\theta_2}\mathrm{e}^{-\mathrm{i}(m-n)(\frac{\pi}{2}-\alpha_{\mathrm{s}})})\right] +$$
$$\mu_{\mathrm{s}}\left[\sum_{n=-N}^{N} A_{\mathrm{o}3,n} \sum_{m=-M}^{M} (k_{\beta\mathrm{s}} \mathrm{J}'_m(k_{\beta\mathrm{s}} r_2)\mathrm{H}_{m-n}^{(1)}(k_{\beta\mathrm{s}} * 2R\cos(\alpha_{\mathrm{s}}))\mathrm{e}^{\mathrm{i}m\theta_2}\mathrm{e}^{-\mathrm{i}(m-n)(\frac{\pi}{2})})\right] +$$
$$\mu_{\mathrm{s}}\left[\sum_{n=-N}^{N} A_{\mathrm{o}2,n} k_{\beta\mathrm{s}} \mathrm{H}_n'^{(1)}(k_{\beta\mathrm{s}} r_2)\mathrm{e}^{\mathrm{i}n\theta_2}\right]_{r_2=a\mathrm{f}2} \quad \text{(A27)}$$

Satisfying boundary condition B.4:

According to boundary condition B.4 (Eq. A18), we need to transfer all necessary waves from their original coordinate system to coordinate system #2. Using that, and considering boundary condition B.4, leads to

$$\left[\sum_{n=-N}^{N} A_{i2,n} \mathrm{J}_n(k_{\beta\upsilon} r_2)\mathrm{e}^{\mathrm{i}n\theta_2}\right] -$$
$$\left[\sum_{n=-N}^{N} A_{o3,n} \sum_{m=-M}^{M} (\mathrm{J}_m(k_{\beta\mathrm{s}} r_2)\mathrm{H}_{m-n}^{(1)}(k_{\beta\mathrm{s}} * 2R\cos(\alpha_{\mathrm{s}}))\mathrm{e}^{\mathrm{i}m\theta_2}\mathrm{e}^{-\mathrm{i}(m-n)(\frac{\pi}{2})})\right] -$$
$$\left[\sum_{n=-N}^{N} A_{\mathrm{sc},n} \sum_{m=-M}^{M} (\mathrm{J}_m(k_{\beta\mathrm{s}} r_2)\mathrm{H}_{m-n}^{(1)}(k_{\beta\mathrm{s}} R)\mathrm{e}^{\mathrm{i}m\theta_2}\mathrm{e}^{-\mathrm{i}(m-n)(\frac{\pi}{2}-\alpha_{\mathrm{s}})})\right] -$$
$$\left[\sum_{n=-N}^{N} A_{\mathrm{o}2,n} \mathrm{H}_n^{(1)}(k_{\beta\mathrm{s}} r_2)\mathrm{e}^{\mathrm{i}n\theta_2}\right]_{r_2=a\mathrm{f}2} = f_1(\theta_2)$$

(need period here) (A28)

Satisfying boundary condition B.5:

According to boundary condition B.5 (Eq. (A19)), we need to transfer all necessary waves from their original coordinate system to coordinate system #3. Using that, and considering boundary condition B.5, leads to

$$\mu_{\mathrm{s}}\left[\sum_{n=-N}^{N} A_{i3,n} k_{\beta\mathrm{s}} \mathrm{J}'_n(k_{\beta\mathrm{s}} r_3)\mathrm{e}^{\mathrm{i}n\theta_3}\right]_{r_3=a\mathrm{f}3} =$$
$$\mu_{\mathrm{s}}\left[\sum_{n=-N}^{N} A_{\mathrm{sc},n} \sum_{m=-M}^{M} (k_{\beta\mathrm{s}} \mathrm{J}'_m(k_{\beta\mathrm{s}} r_3)\mathrm{H}_{m-n}^{(1)}(k_{\beta\mathrm{s}} R)\mathrm{e}^{\mathrm{i}m\theta_3}\mathrm{e}^{-\mathrm{i}(m-n)(\frac{3\pi}{2}+\alpha_{\mathrm{s}})})\right] +$$
$$\mu_{\mathrm{s}}\left[\sum_{n=-N}^{N} A_{\mathrm{o}2,n} \sum_{m=-M}^{M} (k_{\beta\mathrm{s}} \mathrm{J}'_m(k_{\beta\mathrm{s}} r_3)\mathrm{H}_{m-n}^{(1)}(k_{\beta\mathrm{s}} * 2R\cos(\alpha_{\mathrm{s}}))\mathrm{e}^{\mathrm{i}m\theta_3}\mathrm{e}^{-\mathrm{i}(m-n)(\frac{3\pi}{2})})\right] +$$
$$\mu_{\mathrm{s}}\left[\sum_{n=-N}^{N} A_{\mathrm{o}3,n} k_{\beta\mathrm{s}} \mathrm{H}_n'^{(1)}(k_{\beta\mathrm{s}} r_3)\mathrm{e}^{\mathrm{i}n\theta_3}\right]_{r_3=a\mathrm{f}3} \quad \text{(A29)}$$

Satisfying boundary condition B.6:

According to boundary condition B.6 (Eq. (A20)), we need to transfer all necessary waves from their original coordinate system to coordinate system #3. Using that, and considering boundary condition B.6, leads to

$$\left[\sum_{n=-N}^{N} A_{i3,n} \mathrm{J}_n(k_{\beta\upsilon} r_3)\mathrm{e}^{\mathrm{i}n\theta_3}\right] -$$
$$\left[\sum_{n=-N}^{N} A_{\mathrm{o}2,n} \sum_{m=-M}^{M} (\mathrm{J}_m(k_{\beta\mathrm{s}} r_3)\mathrm{H}_{m-n}^{(1)}(k_{\beta\mathrm{s}} * 2R\cos(\alpha_{\mathrm{s}}))\mathrm{e}^{\mathrm{i}m\theta_3}\mathrm{e}^{-\mathrm{i}(m-n)(\frac{3\pi}{2})})\right] -$$
$$\left[\sum_{n=-N}^{N} A_{\mathrm{sc},n} \sum_{m=-M}^{M} (\mathrm{J}_m(k_{\beta\mathrm{s}} r_3)\mathrm{H}_{m-n}^{(1)}(k_{\beta\mathrm{s}} R)\mathrm{e}^{\mathrm{i}m\theta_3}\mathrm{e}^{-\mathrm{i}(m-n)(\frac{3\pi}{2}+\alpha_{\mathrm{s}})})\right] -$$
$$\left[\sum_{n=-N}^{N} A_{\mathrm{o}3,n} \mathrm{H}_n^{(1)}(k_{\beta\mathrm{s}} r_3)\mathrm{e}^{\mathrm{i}n\theta_3}\right]_{r_3=a\mathrm{f}3} = f_2(\theta_3) \quad \text{(A30)}$$

In Eqs. (A26)–(A30), the characters R and α_{s} are defined as follows:

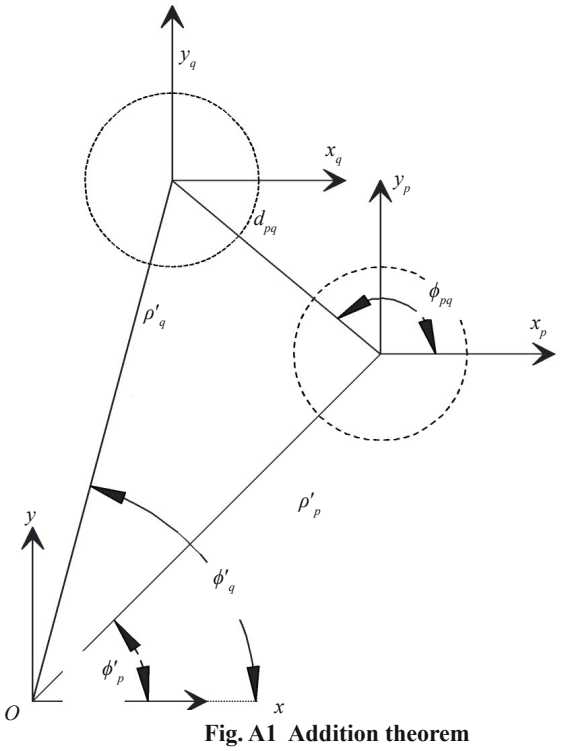

Fig. A1 Addition theorem

$$\left\{\begin{array}{l} R=(\alpha_{f1}^2+\alpha_{f2}^2-2\alpha_{f1}\alpha_{f2}\cos(\beta_1))^{\frac{1}{2}} \\ \beta_1=\dfrac{\pi}{2}+\alpha_{f1}+\alpha_{f2} \\ \beta_2=\arccos(\dfrac{R^2+\alpha_{f1}^2-\alpha_{f2}^2}{2\alpha_{f1}R}) \\ \alpha_s=\alpha_{f1}+\beta_2 \end{array}\right\} \quad \text{if}: 0\le\alpha_{f2}<\frac{\pi}{2}-\alpha_{f1} \tag{A31}$$

$$\left\{\begin{array}{l} R=(\alpha_{f1}^2+\alpha_{f2}^2-2\alpha_{f1}\alpha_{f2}\cos(\beta_1))^{\frac{1}{2}} \\ \beta_1=\dfrac{3\pi}{2}-\alpha_{f1}-\alpha_{f2} \\ \beta_2=\arccos(\dfrac{R^2+\alpha_{f1}^2-\alpha_{f2}^2}{2\alpha_{f1}R}) \\ \alpha_s=\alpha_{f1}-\beta_2 \end{array}\right\} \quad \text{if}: \frac{\pi}{2}-\alpha_{f1}\le\alpha_{f2}<\frac{3\pi}{2}-\alpha_{f1} \tag{A32}$$

$$\left\{\begin{array}{l} R=(\alpha_{f1}^2+\alpha_{f2}^2-2\alpha_{f1}\alpha_{f2}\cos(\beta_1))^{\frac{1}{2}} \\ \beta_1=\dfrac{-3\pi}{2}+\alpha_{f1}+\alpha_{f2} \\ \beta_2=\arccos(\dfrac{R^2+\alpha_{f1}^2-\alpha_{f2}^2}{2\alpha_{f1}R}) \\ \alpha_s=\alpha_{f1}+\beta_2 \end{array}\right\} \quad \text{if}: \frac{3\pi}{2}-\alpha_{f1}\le\alpha_{f2}<2\pi \tag{A33}$$

Also, to satisfy the boundary conditions we should use Fourier and inverse Fourier transform of $f(\theta)$ to model $f_1(\theta_2)$ and $f_2(\theta_3)$, as follows:

$$f_n=\frac{1}{2\pi}\int_0^{2\pi} f(\theta)e^{-in\theta}d\theta \tag{A34}$$

$$f_n=\begin{cases} \left\{\begin{array}{l}\dfrac{i}{2\pi}[H(2\pi-\alpha_1)(e^{-2in\pi}-e^{-in\alpha_1})+H(-\alpha_1)(e^{-in\alpha_1}-1) \\ -H(2\pi-\alpha_2)(e^{-2in\pi}-e^{-in\alpha_2})-H(-\alpha_2)(-e^{-in\alpha_2}+1)]\end{array}\right\} & \text{if}: n\neq 0 \\ \left\{\begin{array}{l}\dfrac{1}{2\pi}[H(2\pi-\alpha_1)(2\pi-\alpha_1)+H(-\alpha_1)(\alpha_1) \\ -H(2\pi-\alpha_2)(2\pi-\alpha_2)-H(-\alpha_2)(\alpha_2)]\end{array}\right\} & \text{if}: n=0 \end{cases} \tag{A35}$$

Since $0<\alpha_1<\alpha_2<2\pi$, f_n becomes:

$$f_n=\begin{cases} \dfrac{i}{2\pi}(e^{-in\alpha_2}-e^{-in\alpha_1}) & \text{if}: n\neq 0 \\ \dfrac{1}{2\pi}(\alpha_2-\alpha_1) & \text{if}: n=0 \end{cases} \tag{A36}$$

The inverse of the Fourier transform can be written as

$$f(\theta)=\sum_{n=-N}^{N} f_n e^{in\theta} \tag{A37}$$

Then, $f_1(\theta_2)$ and $f_2(\theta_3)$ can be derived using Eq. (23).

Equations (A26)–(A30) above have to hold for all θ, and all coefficients of $e^{in\theta}$ have to be equal to zero independently for all integer values of n from $-N$ to $+N$. Thus, $5N+10$ linear equations are obtained to calculate $10N+5$ unknown constants.